Model for incipient triple point in krypton and nitrogen adsorbed on graphite

K. J. Niskanen and R. B. Griffiths
Carnegie-Mellon University, Pittsburgh, Pennsylvania 15213
(Received 21 February 1985)

An anomaly which occurs in the submonolayer phase diagram of krypton and nitrogen adsorbed on graphite has been ascribed to an "incipient triple point" arising because the low free energy of the solid phase of the adsorbed film prevents the occurrence of a liquid phase. In this paper a detailed thermodynamic model for an incipient triple point is developed and applied to these two systems. The model employs a two-dimensional Ising lattice gas for the fluid phase and a fairly simple phenomenological expression for the free energy of the solid phase, which is assumed to be inert. The parameters are adjusted to fit the experimental heat-capacity data with the use of a method which permits a separate determination of the parameters for the fluid and solid phases. The results are in reasonably good agreement with experiment except for some systematic deviations at higher temperatures and coverages which may reflect the inadequacy of a lattice-gas free energy for the fluid. The parameters of the fluid phase, in particular the metastable critical temperature, are physically reasonable and do not seem to be seriously affected by the influence of substrate imperfections on the experimental results. As the thermodynamic model is a model of the free energy, all thermodynamic properties can be computed once the model parameters are chosen. The changes in the phase diagram and in the specific heat as the parameters are varied, are considered in a simple case in order to explore what happens as a triple point changes into an incipient triple point at a critical endpoint.

I. INTRODUCTION

The physics of adsorbed monolayers has attracted much interest in recent years.[1-3] The phase transitions in these two-dimensional systems differ in many respects from their three-dimensional counterparts. A particular anomaly occurs in krypton[4] and nitrogen[5,6] adsorbed on graphite, where no liquid-gas phase separation is found. Instead there is a region in the supermonolayer phase diagram where a solid coexists with a fluid phase whose density (or coverage) varies smoothly, though rapidly, with temperature. There is no liquid phase coexisting with a gas phase, and thus no critical point or triplet point.

In this paper we develop a phenomenological model of the free energy of submonolayer films and apply it to krypton and nitrogen on graphite. Depending on the values of its parameters the model leads either to the usual phase diagram with a triple point and a critical point, or to one with no triple point or critical point. In the latter case the system has an "incipient triple point."[4] We adjust the model parameters via a thermodynamic analysis of the specific heat measured for krypton[4] and nitrogen[5,6] adsorbed on graphite. We find that the model with an incipient triple point is in good agreement with the experiments, and thus the incipient-triple-point explanation seems to be correct for these two systems.

Thomy and Duval[7] interpreted their vapor-pressure-isotherm measurements of krypton on graphite as indicating the presence of both a triple point and a critical point with liquid-gas coexistence in between. However, Larher[8] in a later study concluded that the triple and critical points were very close together, and Butler *et al.*,[4] on the basis of specific-heat measurements, proposed that there is no liquid-gas coexistence in this system, but only an incipient triple point. The mechanism by which an incipient triple point can arise is that the corrugation of the graphite substrate favors the commensurate solid phase of krypton over the liquid, and the liquid-gas phase separation is therefore preempted by solidification. In contrast, in the case of an incommensurate solid phase the corrugation does not stabilize the solid phase in any obvious way, and the usual liquid-gas phase separation occurs, as observed in, for example, xenon[7,9] and methane[10] on graphite.

The measured specific heat of krypton on graphite has a strong peak in the solid-fluid coexistence region at the temperature where the density of the fluid phase coexisting with the solid varies rapidly. The lever rule implies that in this region solid is rapidly converted into fluid when temperature is increased. The anomaly in the specific heat corresponds to this rapid but continuous melting of the solid, in the same way as the delta-function peak at an ordinary triple point arises from the abrupt melting.

Butler *et al.*[4] found that their results were generally consistent with a simple model of the incipient triple point, aside from the fact that at high coverages the maximum in the measured specific-heat peak shifted to higher temperatures, whereas the model predicted that it should stay at the same temperature. They thought that this shift might reflect a finite-size effect, whereas we shall show that a more realistic model allows for such a shift on an ideal substrate (i.e., an infinite graphite surface without defects).

Nitrogen on graphite closely resembles krypton. At the temperatures of interest the molecules are rotating and are

roughly spherical[5] with an average radius about equal to that of krypton. The same "$\sqrt{3}\times\sqrt{3}$" commensurate solid phase is found in both krypton[11,12] and nitrogen[13,14] on graphite, and the specific-heat measurements by Migone and Chan[5,6] show no evidence of a liquid phase in a submonolayer film of nitrogen.

In a preliminary model analysis of the data of Migone and Chan we found[5] that the specific-heat results agreed reasonably well with the incipient-triple-point mechanism. However, in the model the fluid phase was approximated by scaling expressions, valid asymptotically close to a critical point, but the fit to the experimental data implied that the metastable critical point is some 20% below the temperatures of interest. Therefore, an improved analysis was clearly called for. This paper reports the results of such an analysis.

Recent density-functional calculations by Sander and Hautman[15] support the physical basis of the incipient-triple-point explanation. In the calculations the effect of the corrugation of the adsorption potential is taken into account explicitly. Good agreement is found with the experimental phase diagrams of krypton and nitrogen on graphite.

A different explanation for the absence of the liquid-gas phase separation in krypton (and nitrogen) on graphite was proposed by Ostlund and Berker,[16] who argued that on an ideal substrate a first-order transition from solid to gas at low temperatures would change into a continuous-melting transition at a tricritical point (at 78 K in the case of krypton). In real systems, however, the tricritical point and the continuous-melting line close to it would be smeared out by finite-size effects and temperature inhomogeneities. This would give rise to a phase diagram where there would appear to be a solid-fluid coexistence region of the sort observed in the specific-heat measurements with an apparent tricritical point at a significantly higher temperature. We will comment on this alternative in Sec. VI.

The outline for the rest of this paper is the following. We start by discussing, in Sec. II, the physical mechanism of an incipient triple point. We show how an increase in the stability of the solid in general suppresses liquid-gas phase separation and leads to what we call an incipient triple point. We then define our model using separate expressions for the free energies of fluid and solid phases. The fluid phases are described by an Ising lattice-gas model, but in addition some alternative models are considered. The free energy of the solid is taken to be a completely phenomenological smooth function of temperature and coverage.

In Sec. III we fit the parameters of our model to the specific-heat data of nitrogen obtained by Migone and Chan.[5,6] A thermodynamic procedure allows the parameters of the fluid model to be fitted first, independently of the parameters of the solid model. The latter can then be adjusted separately. In addition, the data of Chung and Dash[17] are used to study how sensitive the parameters of the (fluid) model are to the influence of substrate imperfections on the experimental data.

The specific heat data of krypton[4] is treated in Sec. IV. The procedure of Sec. III is shown to work in this case as well. In Sec. V the parameters of our model are varied to explore what happens as one goes from the case of an actual triple point to the case of an incipient triple point. A summary of the paper is given in Sec. VI.

II. THERMODYNAMIC MODEL

We describe the behavior of the submonolayer film using a model of the Helmholtz free energy in which the fluid and solid free energies are given by separate expressions. This approach is reasonable if the solid phase does not become critical simultaneously with the fluid phase. (Both nitrogen and krypton on graphite have solid-fluid tricritical points, but at temperatures well above those of interest here.)

Before the details of the model we illustrate how the incipient-triple-point phase diagram arises from such a model. A graphical model of the Helmholtz free energy per unit area as a function of coverage is shown in Fig. 1. The diagrams on the left-hand side depict the free energy at four different temperatures for a system with an ordinary triple point and the diagrams on the right show the free energy at the same temperatures as on the left, but for a system with an incipient triple point. In each of the diagrams the solid and fluid phases are described by separate free-energy wells, the one on the left (low coverages) being that of the fluid and the one on the right (high coverages) that of the solid.

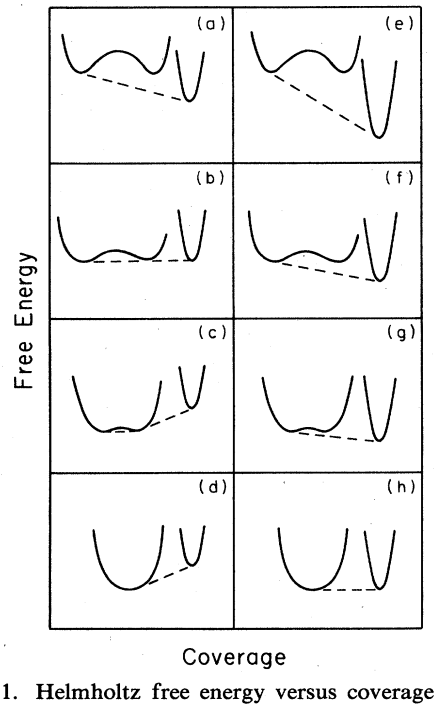

FIG. 1. Helmholtz free energy versus coverage at different temperatures for a system with an ordinary [(a)—(d)] and an incipient triple point [(e)—(h)]. In diagram (a) the temperature is below the triple point, $T < T_t$; in (b), $T = T_t$; in (c), $T_c > T > T_t$; and in (d), $T > T_c$. Diagrams (e)—(h) differ from the adjacent diagrams on the left only in that the free energy of the solid is lower.

The equilibrium free energy of the system has to be a convex function of coverage. This is enforced by the double-tangent construction, indicated by the dashed lines in the figure. The double tangent gives the free energy of the system when it is decomposed into two separate phases, the coverages of which are given by the tangent points. The exact free energy, if known, would correspond to the convex envelope.

Let us first consider the sequence of diagrams (a)—(d) on the left-hand side of Fig. 1, where temperature increases from (a) to (d). The fluid free energy well shows the transition from liquid-gas coexistence at low temperatures to a homogeneous fluid phase above the critical point. The solid free-energy well, on the other hand, is narrow (the solid is relatively incompressible) and in this simplified discussion can be taken to have a temperature-independent shape.

Figure 1(a) depicts the situation below the triple point, $T<T_t$. Thus, in addition to the gas and solid phases, there is a substantial interval, in coverage, of solid-gas coexistence. As temperature increases the free energy of the fluid decreases relative to that of the solid because the solid has less entropy than the fluid. As a result the coverage of the gas coexisting with solid increases. Then at some particular temperature the solid-gas double tangent meets the liquid free-energy well [Fig. 1(b)]. This is the triple point $T=T_t$, where all the three phases coexist simultaneously. When the temperature is further increased the tangent breaks into two, the one at high coverages corresponding to solid-liquid coexistence and the one at lower coverages to liquid-gas coexistence [Fig. 1(c)]. Above the critical temperature [Fig. 1(d)] only the solid-liquid coexistence remains. It is easy to confirm that the sequence (a) to (d) gives rise to the usual phase diagram of three-dimensional matter.

Next we consider the sequence of diagrams (e) to (h) on the right-hand side in Fig. 1 and show that it leads to an incipient triple point. The diagrams differ from the adjacent diagrams on the left only in that the free energy of the solid is lower on the right. As a result quite a different phase diagram arises.

At low temperatures the shift in the free energy of the solid does not have much effect on the solid-gas coexistence. The coverages of the coexisting phases are almost the same in Figs. 1(a) and 1(e). At higher temperatures, however, the change in the solid free energy has more effect. At the temperature where there was previously a triple point (b), the liquid now has a larger free energy than the coexisting gas and solid [Fig. 1(f)]. Consequently, the liquid phase cannot be observed.

In the case illustrated here the free energy of the solid continues to be lower than that of the fluid phases all the way up to a temperature above the critical point [Fig. 1(h)]. Thus only one coexistence region of solid and fluid is observed. In all the diagrams (e) to (h) the coverage of the fluid at the phase boundary is lower than (or equal to) the critical coverage, while coverages characteristic of a liquid would be observed coexisting with the solid at still higher temperatures. On the other hand, there is no clear distinction between gas and liquid at the phase boundary, so that the coverage of the fluid varies smoothly with temperature. Note how a lowering of the free energy of the solid phase has suppressed the liquid-gas phase separation. If the situation in diagram (h) occurs not too far above the critical temperature, the fluid-to-coexistence phase boundary increases rapidly with temperature as the double tangent sweeps across the broad minimum of the fluid free-energy well.

We now consider in more detail the models of the fluid and the solid. The fluid phases are described by an Ising lattice gas in which we ignore the effects of the substrate corrugation that, according to the density-functional studies,[18] mainly affects the commensurate solid phase. Thus the lattice of the lattice-gas model has no relation to the structure of the substrate. The lattice-gas approximation was chosen since no realistic and practical equation of state is available for the two-dimensional fluid, and in fact even the correct form of the interactions between adsorbed atoms is not quite clear.[19]

The Helmholtz free energy per unit area of the fluid, $\phi(n,T)$, is related to the standard (Gibbs) free energy of the Ising model, $G(T,H)=-k_BT\ln(Z)/N$, via

$$\phi(n,T)=G(T,H)+\mu(n-n_c)\ . \tag{1}$$

We make the identification of the Ising magnetization $m=-\partial G/\partial H$ with $(n-n_c)/n_c$, where n_c is coverage of the (metastable) critical point, and the Ising magnetic field H with the chemical potential μ through

$$\mu=H/n_c\ . \tag{2}$$

The scale of n is chosen so that $n=1$ corresponds to the complete registered monolayer. The chemical potential μ is given by

$$\mu=\frac{\partial\phi(n,T)}{\partial n}\ . \tag{3}$$

Note that $\phi(n,T)$ is completely defined by Eq. (1) when the critical temperature T_c and critical coverage n_c are given because the exchange constant of the Ising model determines T_c. We should, in principle, have added a term of the form $n\phi_0(T)$ in Eq. (1) and $\phi_0(T)$ in Eq. (2), because the model as defined does not contain all the ideal-gas degrees of freedom. However, we can subtract the "ideal-gas" contribution to the specific heat from the measured values to obtain a *reduced* specific heat to which our model is then fitted.

The free energy $G(T,H)$ of the Ising model has to be evaluated numerically. In a preliminary study[5] that employed a scaling expression for $G(T,H)$, we found that for nitrogen on graphite the critical temperature appears to be some 20% below the interesting temperature range. Therefore in this temperature range the asymptotic scaling properties cannot provide an accurate equation of state for the fluid.

We have chosen to work with the variational renormalization-group method of Kadanoff.[20,21] It is straightforward to implement and, to the best of our knowledge, yields better accuracy than any other existing practical computational scheme. We use a slightly modified version of the original scheme with the variational parameter p taken as a predetermined function of tem-

perature rather than being optimized at each iteration. The scheme yields the thermodynamic properties of the Ising model on both square and triangular lattices. Most of our calculations are done with the triangular Ising model. Details of the scheme, including estimates of its accuracy, can be found in the Appendix.

In addition to the Ising lattice gas we consider two other fluid equations of state, the mean-field lattice-gas model and the van der Waals model. In the mean-field case $\phi(n,T)$ is defined by

$$\phi(n,T)=-k_BT\ln(1-m^2)/2 + mk_BT\ln\left[\frac{1+m}{1-m}\right]-3k_BT_cm^2/2\ , \quad (4)$$

with $m=(n-n_c)/n_c$, and in the van der Waals model case, by

$$\phi(n,T)=-an^2-nk_BT\ln(n^{-1}-b)\ , \quad (5)$$

with $a=9k_BT_c/8n_c$ and $b=(3n_c)^{-1}$. Note that for the lattice-gas models n is restricted to lie between 0 and $2n_c$ as a result of the special symmetry, whereas for the van der Waals model the domain of n ranges from 0 to $b^{-1}=3n_c$.

The commensurate solid phase is expected to have a small compressibility and it should show no thermal expansion. We approximate the free energy of the solid phase by a phenomenological smooth function of coverage and temperature defined as

$$\psi(n,T)=\psi_0(T)+\psi_1(T)x+p(x)\ , \quad (6)$$

where

$$x=n-n_0 \quad \text{with } n_0=1.0\ , \quad (7)$$

$\psi_0(T)$ and $\psi_1(T)$ are smooth functions of temperature,

$$\psi_r(T)=\sum_{i=0}^{2}\psi_{r,i}(T-T_0)^i,\quad r=0,1 \quad (8)$$

and T_0 is a suitable reference temperature. The function $p(x)$ is

$$p(x)=(x-x_m)^2[p_2+p_3x+p_4x^2+p_s/(x-x_s)^2]\ , \quad (9)$$

where the singular term is helpful in fitting the data, but the pole has no physical significance: x_s is chosen outside the range of coverages that are relevant in our study, and in any case $p(x)$ does not appear directly in the specific heat of the solid.

Despite its complicated appearance, Eq. (6) is a relatively simple expression. The first two terms allow for a specific heat which can vary linearly with the coverage. The $p(x)$ term gives the compressibility of the solid, which is thus assumed to be temperature independent. Since the compressibility is positive, $p(x)$ must be a convex function. If $p(x)$ were a parabola the compressibility would be independent of coverage, but this is inconsistent with our fit of the experimental results.

Finally the free energy $f_{||}(n,T)$ within the coexistence region is given by the double tangent construction as

$$f_{||}(n,T)=\phi(n_1,T)+\mu_{||}(T)(n-n_1)$$

or (10)

$$f_{||}(n,T)=\psi(n_2,T)+\mu_{||}(T)(n-n_2)\ ,$$

where $n_1(T)$ and $n_2(T)$ are the fluid-to-coexistence and solid-to-coexistence phase boundaries. The free energy of the system consists of $\phi(n,T)$ for $n\le n_1$, $f_{||}(n,T)$ for $n_1\le n\le n_2$, and $\psi(n,T)$ for $n\ge n_2$.

III. ANALYSIS OF THE NITROGEN DATA

A. Phase boundaries and "background" correction

Our model analysis relies to some extent on the experimental phase boundaries. We therefore start by discussing the information that can be inferred directly from the experiments. The specific-heat traces measured by Migone and Chan[22] are displayed in Fig. 2 as the dots. (The solid lines are results of our model calculation, to be discussed below.) The transition from solid-fluid coexistence to fluid can be easily distinguished since it corresponds to a drop—discontinuous in the ideal case—in the specific heat with increasing temperature. The scatter of the data is fairly small and the phase boundary n_1 can thus be pinned down quite accurately. The result is shown in Fig. 3.

The transition between solid and solid-fluid coexistence, on the other hand, is difficult to observe. This is because the phase boundary $n_2(T)$ is presumably almost parallel to the temperature axis and thus to the constant coverage scans of the experiment, which implies that the specific-heat discontinuity at this boundary is also small. Therefore random scatter and imperfections of the experimental sample (e.g., finite-size effects), even if very small, can round the discontinuity at the boundary. Fairly tight bounds for the boundary n_2 can, however, be inferred in the following way. In the two-phase region the specific heat $C_{||}(n,T)$ is a linear function of coverage:

$$C_{||}(n,T)=C_{||}(n_1,T)-(n-n_1)Td^2\mu_{||}/dT^2 =C_{||}(n_2,T)-(n-n_2)Td^2\mu_{||}/dT^2\ , \quad (11)$$

where $C_{||}(n_1,T)$ and $C_{||}(n_2,T)$ are the two-phase specific heat along the phase boundaries [cf. Eq. (20) below]. We can evaluate the slope, $-\partial C_{||}/\partial n=Td^2\mu_{||}/dT^2$, in the region where the linear coverage dependence is unambiguous and extrapolate the specific heat from this linear regime to higher coverages. This extrapolation is given by the dashed line in Fig. 2 at the three highest coverages measured, $n=0.955$, 0.975, and 1.01.

At $n=0.955$ we conclude that the measurement is consistent with two-phase coexistence, at least up to 53 K. At $n=1.01$, just above the nominal coverage $n=1.00$ of the complete registered monolayer, no anomaly is observed from 44 to 60 K. The measured specific heat is constant, in accord with the assumption of an inert solid phase. Thus the phase boundary should lie between $n=0.955$ and $n=1.01$. At $n=0.975$ a small precursor of a peak is visible below 49 K, whereas above that only the solidlike specific heat is observed. Thus there seems

to be a coexistence-to-solid transition around 49 K at this coverage, and therefore the phase boundary $n_2(T)$ is a decreasing function of temperature. This seems to be the case at least up to 53 K, though eventually the phase boundary should start increasing.

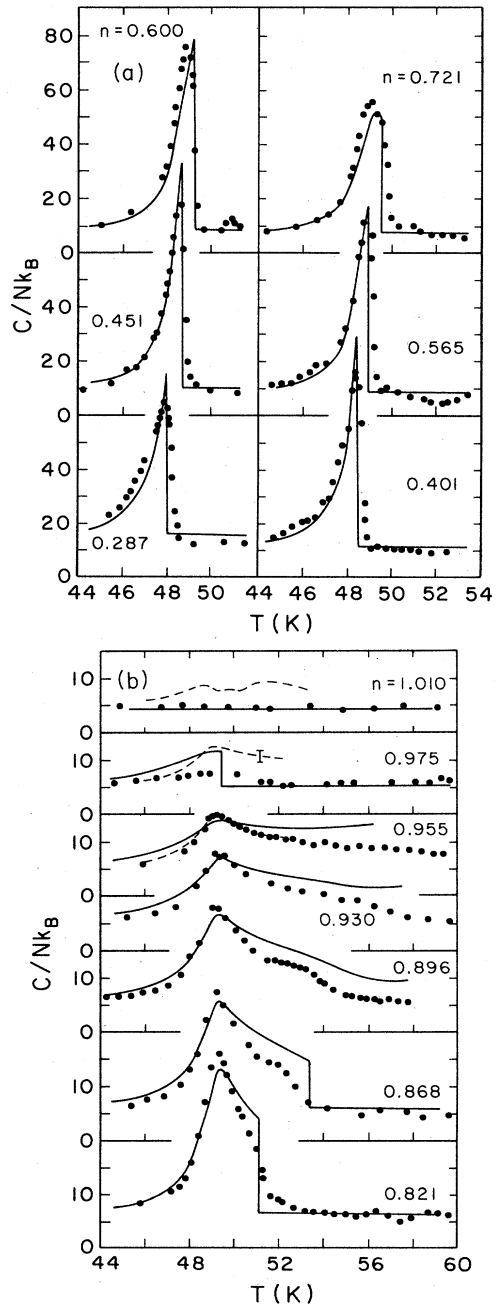

FIG. 2. The specific heat per molecule of nitrogen adsorbed on graphite foam as measured by Migone and Chan at a set of fixed coverages is given by the dots. The final model results are given by the solid lines. The dashed lines at the three highest coverages are inferred from the experimental data (at lower coverages) assuming two-phase coexistence, and the error bar refers to the uncertainty in these values. Note the different vertical scales of the two parts of the figure.

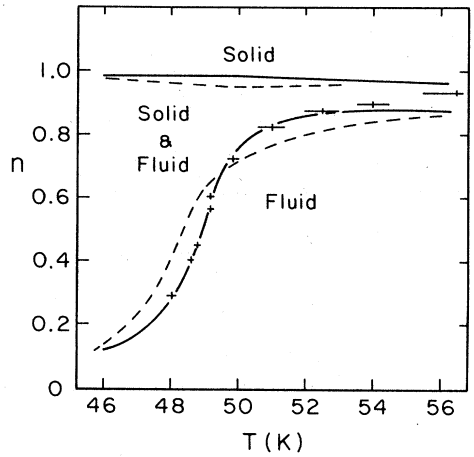

FIG. 3. The submonolayer phase diagram of nitrogen on graphite. The pluses indicate the location of the coexistence-to-fluid phase boundary as inferred from the experiment. The solid lines are the final model results and the dashed lines are the results of Sander and Hautman.

Next we consider the specific heat of the *fluid* film. We estimate that the three-dimensional motion of the nitrogen molecules in the adsorption potential contributes $3k_B$ per molecule at 50 K. In addition to this "ideal-gas" term, the interactions described by the Ising lattice-gas model amount to about $1k_B$ per molecule at $n=\frac{1}{2}$ and to 0 at $n=0$ or 1. However, from Fig. 2 one can see that there is a discrepancy between the expected $(3-4)k_B$ per molecule and the actual measurement. This may represent systematic errors in deducing the film heat capacity from the experimental measurements.[23]

In order to analyze the data and fit them to our model, we have adopted the expediency of subtracting the "background" heat capacity

$$C_0=(3+2n)N_r k_B \ , \tag{12}$$

where N_r is the number of adsorbed atoms at $n=1$, from the experimental data, to yield a reduced heat capacity. The model fits are carried out in terms of the reduced heat capacity. Then at the end of the calculation C_0 is added to the calculated results to yield the curves in Fig. 2. Alternative choices for C_0 are possible, but they will not make much difference except in the pure fluid region where this correction is proportionately large.

B. Fitting the data in the two-phase region

We fitted our model to experimental estimates of the free energy and chemical potential in the solid-fluid coexistence region. The estimates can be obtained by integrating the measured specific heat. We can then fit the models of the fluid and solid phases independently of one another.

The free energy at coexistence [see Eq. (10)], $f_{||}(n,T)$, can be written as

$$f_{||}(n,T)=f_{||}(n_0,T)+\mu_{||}(T)(n-n_0) \ , \tag{13}$$

where $n_0=1.0$ is a convenient reference coverage, and $\mu_{||}(T)$ is the chemical potential at coexistence. An experimental estimate $\mu^e_{||}(T)$ (we use the superscript e to refer to the experimental estimates) is obtained by integrating the slope $-\partial C_{||}/\partial n = T d^2\mu_{||}/dT^2$ [cf. Eq. (11)] of the measured specific heat in the two-phase region:

$$\mu^e_{||}(T)=\mu_q(T)+\mu_0+\mu_1 T \ , \tag{14}$$

where

$$\mu_q(T)=-\int_{T_q}^{T}\int \frac{\partial C_{||}/\partial n}{T} \ , \tag{15}$$

and μ_0 and μ_1 are two undetermined constants of integration. We choose $T_q=46$ K. In order to obtain the corresponding estimate $f^e_{||}(n_0,T)$ for the free energy, we first extrapolate $C_{||}=-T\partial^2 f_{||}/\partial T^2$ up to $n=n_0$ and then integrate twice:

$$f^e_{||}(n_0,T)=f_q(T)+f_0+f_1 T \ , \tag{16}$$

where

$$f_q(T)=-\int_{T_q}^{T}\int \frac{C_{||}(n_0,T)}{T} \ , \tag{17}$$

and f_0 and f_1 are two more constants of integration. The "background" C_0, Eq. (12), is subtracted off before any of the quadratures are carried out.

In what follows we will use the experimental quantities $\mu^e_{||}(T)$ and $f^e_{||}(n_0,T)$ as a basis for independently adjusting the parameters of the fluid and solid models. In the fit of the fluid model the information about the coexisting solid is implicit in $\mu^e_{||}(T)$ and $f^e_{||}(n_0,T)$, and vice versa.

Consider first the adjustment of the parameters of the fluid model. The experimental phase boundary $\mu^e_{||}(T)$ can be combined with the model free energy of the fluid, $\phi(n,T)$, to obtain an estimate $n_1^*(T)$ of the fluid-to-coexistence phase boundary via

$$\mu^e_{||}(T)=\left.\frac{\partial\phi(n,T)}{\partial n}\right|_{n=n_1} . \tag{18}$$

If the fluid model is consistent with the experiment, then $f_1^*(T)$, defined as

$$f_1^*(T)=f^e_{||}(n_0,T)+\mu^e_{||}(T)(n_1^*-n_0)-\phi(n_1^*,T) \ , \tag{19}$$

should vanish within the experimental uncertainty. In addition, $n_1^*(T)$ should be consistent with the phase boundary $n_1^e(T)$ inferred from the experiment. It is important to note that $n_1^*(T)$ and $f_1^*(T)$ depend on both the experimental data and the model of the fluid, but not on the model of the solid.

We can use the two consistency relations, $n_1^*=n_1^e$ and $f_1^*=0$, to adjust the four constants of integration and the parameters of the fluid model, T_c and n_c. The results can be checked by comparing the model prediction of the two-phase specific heat along the phase boundary, $C_{||}(n_1,T)$, with the experimental estimate. In the experiments $C_{||}$ tends to be rounded at the phase boundary. Good estimates can, however, be obtained by extrapolating $C_{||}$ from the region where $C_{||}$ is clearly linear in coverage down to the phase boundary $n_1^e(T)$. The model estimates of $C_{||}(n_1,T)$ are obtained from the equation

$$C_{||}(n_1,T)=-T\phi_{TT}+T\phi_{nn}\left[\frac{dn_1}{dT}\right]^2 , \tag{20}$$

where $\phi(n,T)$ is the model free energy of the fluid, completely determined by T_c and n_c. Then $n_1^*(T)$ is used as an estimate of $n_1(T)$ and the slope of the phase boundary is given by

$$\frac{dn_1}{dT}=\left[\frac{d\mu_{||}}{dT}-\phi_{nT}\right]\Big/\phi_{nn} \ .$$

We then consider the fitting of the solid free energy $\psi(n,T)$ to the experimental data. The information about the fluid equation of state is now implicit in the chemical potential $\mu^e_{||}(T)$ and in the free energy $f^e_{||}(n_0,T)$ at coexistence, determined by the experimental data. We can use the analog of Eq. (18),

$$\mu^e_{||}(T)=\left.\frac{\partial\psi(n,T)}{\partial n}\right|_{n=n_2^*} , \tag{21}$$

to obtain a model-dependent estimate $n_2^*(T)$ of the solid-to-coexistence phase boundary. Unlike the fluid-to-coexistence case, the experimental boundary $n_2^e(T)$ is known only qualitatively and cannot be used in the fit. However we can employ the consistency requirement that $\psi(n,T)$ be equal to $f^e_{||}(n,T)$ along $n=n_2^*(T)$. Since the functional form of the solid free energy is not very obvious in advance, we do not expect to be able to find a reliable representation of the solid outside the immediate neighborhood of the phase boundary.

The solid model $\psi(n,T)$ is given by Eq. (6), with x defined by Eq. (7). Thus $f_2^*(n,T)$, defined as

$$f_2^*(n,T)=f^e_{||}(n_0,T)-\psi_0(T)+[\mu^e_{||}(T)-\psi_1(T)](n-n_0) \ , \tag{22}$$

should be equal to $p(x)$ when $n=n_2^*(T)$. Since the fit of the fluid model discussed previously fixes the integration constants in $f^e_{||}(n_0,T)$ and $\mu^e_{||}(T)$, the condition $f_2^*=p$ determines $\psi_0(T)$ and $\psi_1(T)$.

At any fixed temperature, $f_2^*(n,T)$ is by construction a linear function of coverage. As temperature is varied these straight lines should form an envelope for the *temperature-independent* function $p(x)$. We therefore want to adjust $\psi_0(T)$ and $\psi_1(T)$ so that the corresponding envelope is a convex function of coverage with the functional form of Eq. (9). In addition, $n_2^*(T)$ should satisfy the qualitative conditions inferred from the experimental data. It is the temperature independence of p that allows for the relatively easy and intuitive two-step fitting of the solid model: first the adjustment of $\psi_0(T)$ and $\psi_1(T)$, and then that of $p(x)$. If p depended on temperature, then the notion of an envelope would no longer be useful.

C. Results

Let us now explain the actual choice of parameters. We start with the model of the fluid phase. We have used several methods of adjusting the model parameters n_c and T_c, and the constants of integration μ_0, μ_1, f_0, and f_1. They all lead to similar estimates for n_c and T_c. When

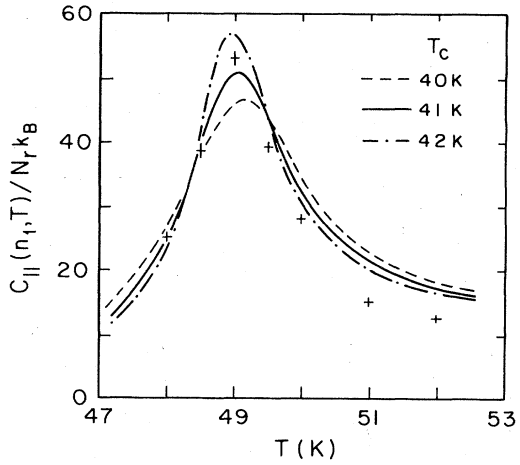

FIG. 4. The two-phase specific heat along the fluid-to-coexistence phase boundary. The pluses give the experimental result and the continuous lines are obtained from the fluid model as explained in the text.

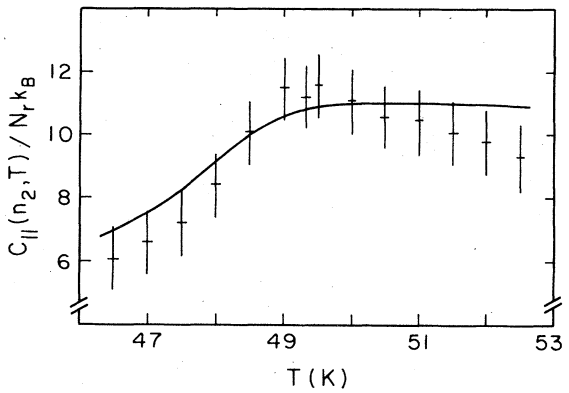

FIG. 5. The two-phase specific heat along the solid-to-coexistence phase boundary. The pluses are obtained by extrapolating the experimental two-phase result up to $n=n_2^*$. The solid curve is the model result.

the critical coverage n_c is chosen between 0.48 and 0.49 and the critical temperature T_c between 40 and 42 K, the consistency requirements $f_1^* \approx 0$ and $n_1^* \approx n_1^e$ are satisfied within the experimental uncertainty. For values of n_c and T_c outside this range the two requirements cannot be satisfied simultaneously.

The model-dependent estimates of the specific heat $C_{||}$ along the phase boundary n_1, shown in Fig. 4, are obtained using the values of the integration constants found earlier with $n_c=0.48$ and $T_c=40$, 41, and 42 K. As one might expect, the peak in the specific-heat curve becomes sharper as T_c becomes larger and the metastable critical point approaches the phase boundary. Both $T_c=41$ and 42 K give equally good agreement with the experiment, which is represented by the pluses. Note that there are no experimental estimates below 48 K because experiments were not carried out at low enough coverages. Overall, the model result is quite good. At high temperatures, however, it clearly overestimates $C_{||}$. We have not been able to eliminate this discrepancy by adjusting the parameters. It will be discussed later. Thus we conclude that our fluid model gives good agreement with the experiment when the model critical temperature is between 41 and 42 K and the critical coverage is 0.48 ± 0.01.

Then consider the adjustment of the solid model. We start by ensuring that the model satisfies the qualitative constraints on the solid-to-coexistence phase boundary: $0.955 < n_2^* < 1.01$, $dn_2^*/dT < 0$, and $n_2^*(T=49\ \text{K}) \approx 0.975$. This can be done by setting $x_m \approx -0.025$, and $\psi_0(T=49\ \text{K})=f_{||}^e(n_0,49\ \text{K})$, $\psi_1(T=49\ \text{K})=\mu_{||}^e(49\ \text{K})$, and, in addition, $d\psi_1/dT$ must be large enough so that $\mu_{||}^e(T)-\psi_1(T)$ [which is equal to dp/dx; cf. Eq. (21)] is a decreasing function of temperature, and, consequently, also $n_2^*(T)$ is a decreasing function of temperature. Another constraint, on $d\psi_0/dT$, ensures the convexity of the envelope.

We still have quite a lot freedom in choosing $\psi_{0,1}$, $\psi_{0,2}$, $\psi_{1,1}$, and $\psi_{1,2}$. In a typical case the envelope formed by f_2^* is quite smooth but asymmetric around the minimum. This asymmetry appears to be a general property, and this is why we have included the pole in the definition of $p(x)$, Eq. (9). The location of the pole x_s is chosen close to zero, and hence the singularity does not directly affect the phase boundary or specific heat at the temperatures of interest. We wish to emphasize that the pole is only a convenient way to parametrize $p(x)$, and does not reflect any physical singularity.

When the parameters in Eq. (9) are properly adjusted, the deviation of $p(x)$ from the envelope is of the same order of magnitude as the experimental uncertainty in $f_2^*(n,T)$ at $n=n_0$. The solid model $\psi(n,T)$ then gives a phase boundary $n_2^*(T)$ that (by construction) satisfies all the conditions discussed above. Also, the two-phase specific heat $C_{||}(n_2^*,T)$, see Fig. 5 for an example, is in reasonable agreement with the experimental estimate obtained by extrapolating the two-phase specific heat to $n=n_2^*(T)$. The agreement could probably be improved by further modifying the model parameters, but this does not seem worthwhile. What we wish to emphasize is that we are able to fit the experimental results with a smooth $\psi(n,T)$ consistent with the absence of any phase transitions *in* the solid phase.

Once all the parameters in the fluid and solid models are determined, one can calculate consistently any thermodynamic quantities of interest. The agreement between the calculated phase boundaries and specific heats can be improved slightly by small modifications in the parameters $\psi_{0,0}$ and $\psi_{0,1}$. Figures 2 and 3 present model results using the final choice of parameter values: $T_c=42$ K, $T_0=49.3$ K, $n_c=0.48$, $\psi_{0,0}=-39.2$ K, $\psi_{0,1}=2.08$, $\psi_{0,2}=0.01\ \text{K}^{-1}$, $\psi_{1,0}=18.9$ K, $\psi_{1,1}=56.8$, $\psi_{1,2}=0.5\ \text{K}^{-1}$, $x_m=-0.0235$, $x_s=-0.01$, $p_2=7.45\times10^3$ K, $p_3=-4.02\times10^4$ K, $p_4=16.3\times10^5$ K, and $p_s=0.46$ K. (In the earlier solid fit, $\psi_{0,0}=-39.3$ K and $\psi_{0,1}=2.15$.)

Let us now discuss the results. First of all, the phase boundaries, the solid curves in Fig. 3, are consistent with the experimental results, except at high temperatures, where the model boundary $n_1(T)$ is a bit low, and is start-

ing to decrease with increasing temperature. This is in disagreement with the experiment and with the fact that the solid is expected to become less stable as temperature increases. Apparently our model fails above 55 K, which is not too surprising, as it should only be valid over a limited temperature interval. The result of Sander and Hautman,[15] the dashed curves in Fig. 3, are included for comparison. Our model result is much better than theirs over the limited temperature range of the figure, whereas the density-functional calculation shows reasonable agreement with the experiment at all temperatures.

Next, consider the model predictions of the specific heat, the solid lines in Fig. 2. There is reasonable agreement in the fluid phase (high-temperature side of the peaks), but this is mostly a matter of having chosen C_0 appropriately. The peak positions are basically correct and the heights are mostly right. At higher coverages the experimental curves show a shoulder on the high-temperature side of the peak, and our calculations produce a qualitatively similar effect, though the final discontinuity is sharper than in the experimental data (which may well be rounded due to finite-size or similar effects). The location of this discontinuity is at too high a temperature at $n=0.868$, reflecting the fact that the model phase boundary is not in the right place, as discussed above. In fact, the model does not give a fluid phase at coverages above $n=0.896$. For coverages of $n=0.868$ and above the model specific heat is too large at temperatures above the peak. On the other hand, the specific heat at temperatures beneath the peak is quite well represented in the model at all coverages.

Reasons have been given in the beginning of this section for supposing that the experimental data indicate a transition from coexistence to solid at the coverage of 0.975. Assuming that this is so, the model specific heat shows a much larger discontinuity than the experiment. The latter may be smoothed out due to the fact that the coexistence-to-solid boundary is almost parallel to the temperature axis. The model gives the correct specific heat on the high-temperature side of this transition and also at $n=1.01$, that is, in the solid phase.

Next we consider the reliability of our model. The model of the solid is completely phenomenological and the parameters given above are based on fitting to the experimental data in the two-phase region. These data depend on the free energy of the solid along the phase boundary from solid to solid-fluid coexistence, and not on the free energy of the solid at higher densities away from this boundary. Thus the model of the solid should not be taken very seriously. The model of the fluid, on the other hand, is quite specific, but contains two approximations. First, the continuum fluid phase is represented by the Ising lattice-gas model, and second, the Ising-model properties are obtained from a renormalization-group approximation.

We now discuss the limitations of the fluid model in more detail. First of all, the triangular symmetry of the Ising model lattice does not seem to play any role in the analysis. We have also employed the square-lattice Ising model in our fits, but found no significant effect on the results. This is reassuring as the real fluid does not have the Ising-lattice symmetry. The fluid has been assumed to be unregistered with respect to the graphite substrate, and thus the substrate effects on the fluid free energy have been neglected. This seems justified, at least at small and intermediate coverages.[18] However, as the fluid coverage increases toward the commensurate coverage, the corrugation of the substrate may become important. It is therefore quite possible that the neglected substrate effects are the reason for the discrepancies seen at higher coverages.

Even in the case of a completely smooth substrate, the lattice-gas model would be misleading in the limit of high coverage. This is because the lattice-gas model is only defined for a coverage range from 0 to $2n_c \approx 1$, but the fluid may well exist at coverages higher than 1.0, at least at high temperatures. Therefore the lattice-gas model has to fail as n approaches 1.0. In particular, at high coverages $-T\phi_{TT}$ is small and $C_{||}(n_1,T)$ is dominated by the second term in Eq. (20):

$$C_{||}(n_1,T) \approx T\phi_{nn}(dn_1/dT)^2 .$$

Since the model result for dn_1/dT is equal to, or smaller than, the experimental result in Fig. 3 (n_1 is roughly correct until it reaches a maximum and starts to decrease), the overestimate of $C_{||}(n_1,T)$ implies that ϕ_{nn} is too large. This is indeed what we would expect from a lattice-gas model, since $\phi_{nn}=\partial\mu/\partial n$ diverges when n approaches its maximum. In real systems $\partial\mu/\partial n$ is always finite.

Kadanoff's variational renormalization-group scheme seems to yield sufficient accuracy for the model fit to make sense. In particular, we find that the uncertainty in our critical-temperature estimate due to approximating the Ising equation of state is less than ± 1 K. The specific heat $C_{||}(n_1,T)$ should be affected by, at most, 10%. The discrepancies with the experimental values, where they are significant, are larger than this.

In summary, the model agrees quite well with the experiment. The most notable exception occurs at high temperatures (or high coverages) where the results seem to be sensitive to the details of the model. It is quite plausible that the discrepancies are due to intrinsic limitations of the lattice-gas model, or the effects of the substrate corrugation.

D. Mean-field and van der Waals equations of state for the fluid

We have found that the specific-heat data for nitrogen can be reproduced by the model if the fluid critical temperature is chosen to be 41 or 42 K. This is some 20% below the region of rapid rise in the phase boundary. It is therefore interesting to see whether the two-dimensional Ising equation of state is really necessary this far from the critical point. We have fitted both the mean-field and the van der Waals equations of state to the experimental data using the same procedures described above. The only difference is that the free energy $\phi(n,T)$ is now given by Eqs. (4) and (5).

The mean-field model tends to give a smoother phase boundary $n_1^*(T)$ for a given T_c than the Ising model. Thus the mean-field estimates of the critical temperature

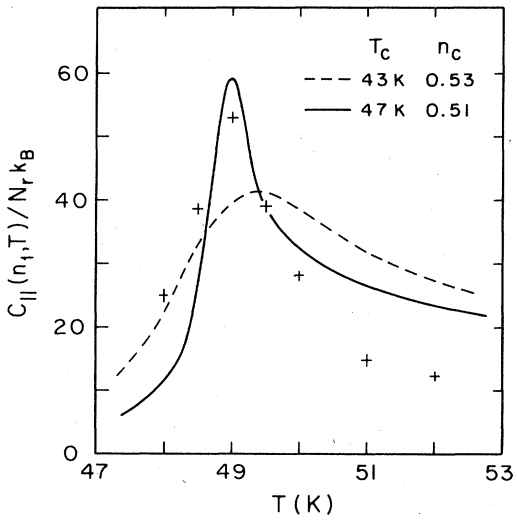

FIG. 6. Specific heat along the phase boundary as in Fig. 4, but with the curves obtained using the mean-field model.

are higher. For $T_c \approx 47$ K, we find $n_1^* \approx n_1^e$ and $f_1^* \approx 0$, though n_1^* does not agree with n_1^e as well as in the Ising case. For lower values of T_c the model phase boundary does not agree with experiment. Figure 6 depicts the two-phase specific heat $C_{||}(n_1^*,T)$ for $T_c = 43$ and 47 K. The critical coverage is chosen so that the model phase boundary agrees with experiment as well as possible. As the critical temperature is increased from 43 to 47 K, the specific-heat curve becomes very asymmetric. On the low-temperature side the specific heat is too small, and on the high-temperature side, too large. Figure 6 should be compared with Fig. 4.

It thus seems that the mean-field approximation is not in as good agreement with the experiment as is the two-dimensional Ising model. The steepness of the measured phase boundary demands a high critical temperature. However, a high T_c leads to an asymmetric specific-heat curve $C_{||}(n_1^*,T)$, which does not agree with the experiment. Thus the phase boundary and the specific heat along it cannot be described as consistently using the mean-field equation of state as they can using the Ising lattice gas.

The van der Waals model for the fluid phase gives even worse results than mean-field theory. It lacks the liquid-gas symmetry of the lattice-gas models, and as real fluids in three dimensions also lack this symmetry, one might have supposed that the van der Waals model would provide a better approximation than mean-field theory for a lattice gas in two dimensions. However, this seems not to be the case.

E. The data of Chung and Dash

Finally, we want to find out how sensitive our analysis is to finite-size and other effects on the experimental data. We compare the nitrogen data of Chung and Dash,[17] obtained with Grafoil as a substrate, with the data of Migone and Chan,[5,6] who used graphite foam as substrate.

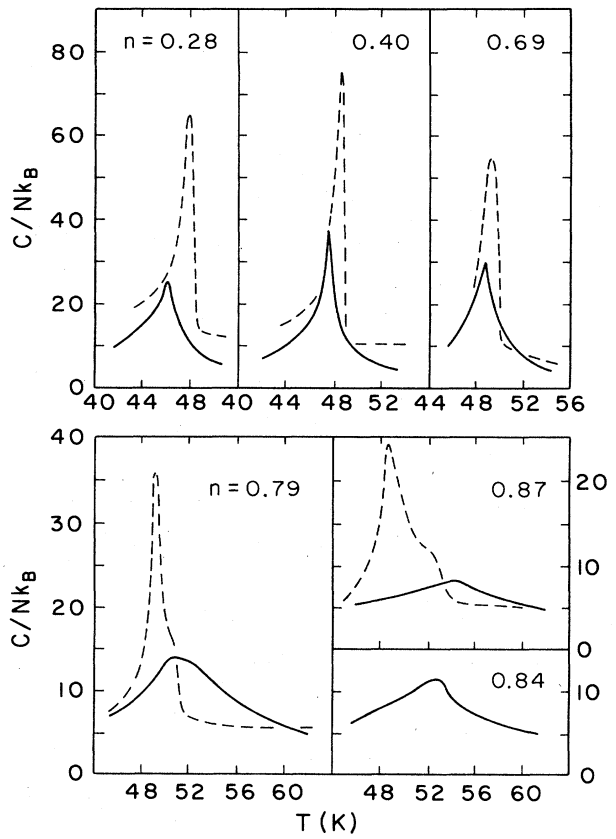

FIG. 7. The specific heat of nitrogen on Grafoil as measured by Chung and Dash (the solid lines). The dashed lines are the results of Migone and Chan at $n = 0.287$, 0.401, 0.721, 0.821, and 0.868. Note the different vertical scales of the top and bottom portions of the figure.

Grafoil is a *recompressed* form of graphite foam with a surface coherence length (size of the surface crystallites) of 100 to 200 Å. This is 5–10 times smaller than the 900 Å characteristic of the foam. Thus we expect substrate imperfections to be more apparent in the data on Grafoil than on graphite foam. However, differences in the macroscopic structure of the substrate material (e.g., proximity effects) and in the experimental techniques may also have induced qualitative differences between the two sets of data. Chung and Dash used a conventional calorimetric technique which is possible because of the compact structure of Grafoil, whereas Migone and Chan[5,6] employed a sensitive ac technique.

Some of the specific-heat data measured by Chung and Dash[24] are displayed in Fig. 7 as solid curves along with the corresponding data of Migone and Chan[22] at approximately the same coverages, shown as dashed curves. The peaks in the Chung-Dash data are smaller and the transition from coexistence to fluid is far less sharp. In general, the peak values are at least 2 times smaller than in the Migone-Chan data. In the high-coverage limit the nominal coverages given by Chung and Dash do not seem to be consistent with the Migone-Chan scale, but some 10% lower. In addition, the peaks in the specific-heat traces of Chung and Dash move to higher temperatures as coverage

increases. This is qualitatively quite different from the data of Migone and Chan, where the peaks stay at $T_0=49.3$ K.

The lower resolution of the Chung-Dash data means that it is not worthwhile trying to fit the parameters of the model of the solid. The model of the fluid, on the other hand, is determined by just two parameters, the critical coverage and the critical temperature. The former is close to 0.5, so that we only need to consider T_c. We find that the specific heat $C_{\|}(n_1^*,T)$ is in fair agreement with the experiment when T_c is between 38 and 42 K. The Migone-Chan data give T_c between 41 and 42 K. Thus the two experiments give consistent results for the critical temperature despite the difference in substrates and experimental techniques. As a consequence, we do not think that our analysis of the Migone-Chan data is seriously affected by the nonideal features of that experiment.

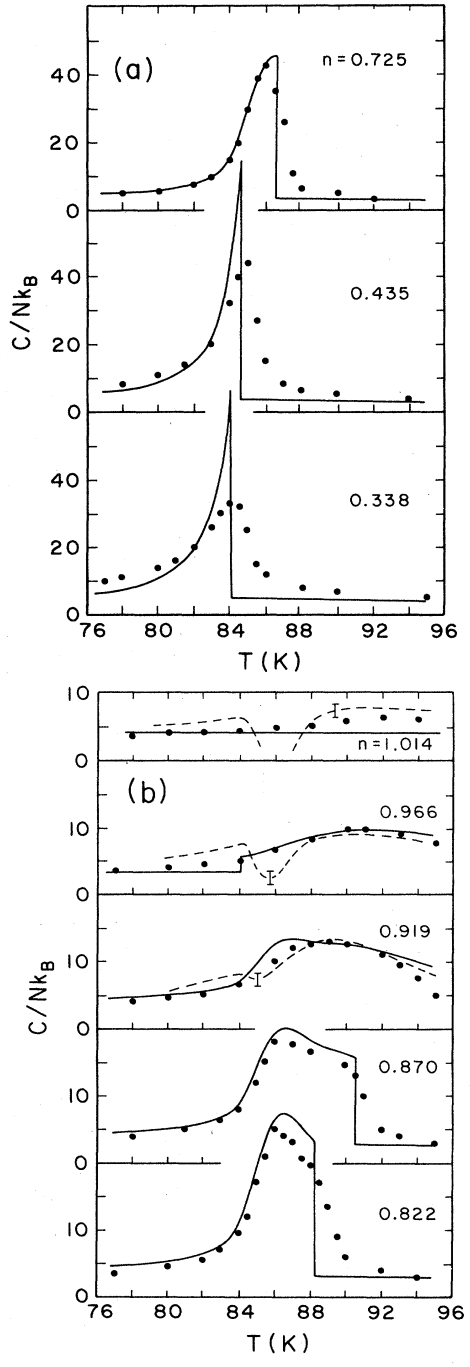

FIG. 8. The dots give the specific heat per krypton atom adsorbed on Grafoil as measured by Butler *et al.* at a set of fixed coverages. The final model results are given by the solid lines. The dashed lines are inferred from the experiment assuming two-phase coexistence at the three highest coverages, and the error bars refer to the uncertainty in these values. Notice the different vertical scales of the two parts.

IV. KRYPTON ON GRAPHITE

A few examples of the specific-heat results of Butler *et al.*[4,25] are shown as points in Fig. 8. (The solid lines are the results of our model calculations to be discussed below.) In each case we have included only a small characteristic subset of the data; random scatter is of the order of $2k_B$ per atom. The traces are more rounded than the analogous results of Migone and Chan, shown in Fig. 2, and in that respect rather similar to those of Chung and Dash, Fig. 7. Both Butler *et al.* and Chung and Dash used Grafoil as a substrate and their experimental techniques were essentially the same. On the other hand, Migone and Chan used the higher-quality graphite-foam substrate and a different method of measurement. Therefore the qualitative differences between the krypton results of Butler *et al.* and the nitrogen results of Migone and Chan may be due to the effects of the substrate or the measuring technique.

Despite the larger rounding of the krypton data most of the results we can infer from them are remarkably similar to those for nitrogen (the data of Migone and Chan). In Fig. 9 we compare the coexistence-to-fluid boundaries and, in Fig. 10, the slopes of the two-phase specific heat

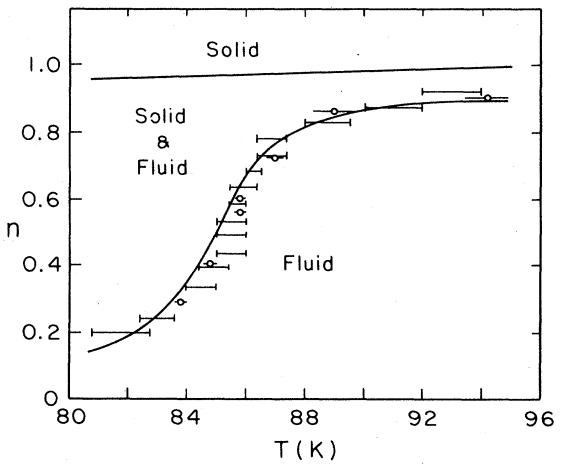

FIG. 9. The submonolayer phase diagram of krypton on graphite. The horizontal bars indicate the location of the coexistence-to-fluid phase boundary as inferred from the experiment. The solid lines are the final model results. The circles with bars are the experimental phase boundary of nitrogen, with the temperatures multiplied by the same constant as in Fig. 10.

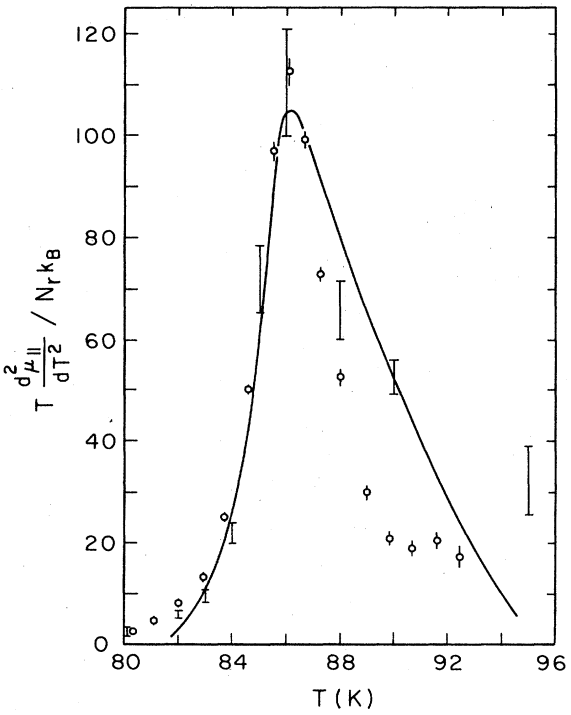

FIG. 10. The slope $-\partial C_{||}/\partial n = Td^2\mu_{||}/dT^2$ of the two-phase specific heat in units of $N_r k_B$, where N_r is the number of atoms at $n=1$. The vertical bars give the experimental result and the solid line the final model result. The nitrogen results are indicated by circles with bars through them, with the temperatures multiplied by a constant to bring the temperatures of the peaks into coincidence.

$(-\partial C_{||}/\partial n = Td^2\mu_{||}/dT^2)$ of the two systems after applying suitable scale factors. In particular, the temperatures for the nitrogen results have been multiplied by a constant to place the peak of $Td^2\mu_{||}/dT^2$ at the same temperature as that for krypton. Well inside the two-phase region, where the rounding of the transition does not seem to affect the data, the krypton specific heat at a fixed temperature is still only roughly linear in coverage, and this is reflected in the fairly large error bars of $-\partial C_{||}/\partial n$. Aside from that, however, the results are very similar to those of nitrogen. Only at the high-temperature end is there some difference between the two results. In the case of the phase boundary, Fig. 9, no real difference can be discerned once the coverage scale has been adjusted as explained below.

The krypton results of Butler *et al.* do differ from the nitrogen results of Migone and Chan when coverage is high. The peak in the specific heat shifts to higher temperatures as the solid phase is approached. This behavior is at least qualitatively the same as that observed in the data of Chung and Dash. It seems therefore that this behavior could be related to the substrate rather than to the adsorbed species. The question of the similarity of nitrogen and krypton on an ideal graphite substrate remains, therefore, unresolved. To our knowledge there is no fundamental reason why the peak in the specific heat could not shift even in the case of an ideal experiment. As will be shown below, our model is indeed consistent with the data of Butler *et al.*, including a shift in this peak, apart from rounding effects.

In Fig. 9 and henceforth we use the convention that $n=n_0=1.0$ is equivalent to the adsorption of 103.5 cm^3 of krypton at STP in Butler's apparatus,[25] which is somewhat different from the coverage scale used by Butler *et al.*, who set $n=1$ to correspond to 120 cm^3. Our choice is motivated by the fact that the solid-to-coexistence transition seems to occur at 100 cm^3, or $n\approx 1.0$ in our units. In analogy to nitrogen it seems plausible that the boundary is located close to the complete registered monolayer. It is possible that as much as 10% of the adsorbed atoms are affected by defects and edges of the substrate crystallites. Therefore discrepancies of the order discussed here in the absolute coverage values are not impossible. We wish to emphasize that the coverage scale is purely a matter of convenience which does not affect our model analysis.

We have estimated the location of the solid-to-coexistence phase boundary from the specific-heat data in the same way as in the nitrogen case. In the coexistence region the specific heat measured at high coverage should agree with a result that is linearly extrapolated from the data at lower coverages. The result of such an extrapolation is shown in Fig. 8 by the dashed line for the three highest coverages. At $n=0.919$ the measurement is consistent with the two-phase coexistence within the uncertainty of the extrapolated values (note the error bar). However, at $n=0.966$ and 1.014 this is not true around $T=86$ K. The data at $n=0.966$ are consistent with coexistence above perhaps 88 K, and for $n=1.014$ the same is true above a somewhat higher temperature. In both of these cases there is evidence of a transition from coexistence to fluid at still higher temperatures, outside the region shown in Fig. 8.

These observations can be explained consistently if the solid-to-coexistence boundary increases in coverage as temperature is increased. At $n=0.966$ and 1.014 the system is then in the solid phase at low temperatures and in the coexistence region above roughly 86 K. The smoothness of the observed data in the region of the purported transition is to be expected since the phase boundary is almost parallel to the constant-coverage paths followed in the experiment. We note that a boundary which decreases monotonically as temperature is increased, as in the case of nitrogen, is not consistent with the high-coverage data. In such a case there should be a decrease of some kind in the specific heat at constant coverage as the boundary is crossed. However, the specific heat is probably affected to some extent by the quality of the substrate. Therefore the apparent increase of the phase boundary as temperature increases may be induced by substrate imperfections.

In fitting our model to the data of Butler *et al.* we follow the procedure of Sec. III. First, we note that the specific heat measured at high temperature in the fluid phase is consistent with our expectation of $2k_B$ per atom in addition to a smaller interaction contribution. Thus $C_0=2Nk_B$ is subtracted from the experimental data, which are subsequently integrated to yield the chemical

potential $\mu_{||}^{e}(T)$ and the free energy $f_{||}^{e}(n_0,T)$ at coexistence; see Eqs. (14) and (16).

The parameters of the fluid model, n_c and T_c, and the constants of integration, are adjusted in the same way as in the nitrogen case. We find that the estimate $n_1^*(T)$ is consistent with $n_1^e(T)$, and $f_1^*(T)\approx 0$, within the uncertainty for a wide range of choices of the critical temperature, from 72 to 78 K. The two-phase specific heat $C_{||}(n_1^*,T)$, on the other hand, is in reasonable agreement with the experiment for T_c between 74 and 76 K. At high temperatures (above 92 K) the model fails, independent of the choice of T_c, perhaps for the same reason as in the case of nitrogen. If T_c is chosen smaller than 73 K or larger than 77 K, the model result of $C_{||}(n_1^*,T)$ will no longer agree with the experimental estimate. However, in view of the experimental uncertainty, it seems better to assign a larger range of T_c from 72 to 78 K. A critical temperature as high as 80 K is definitely inconsistent with the experiments. We use a critical coverage of $n_c=0.49$ in the units we introduced (50.7 cm^3 in Butler's thesis). The value of T_c does not depend sensitively on this choice.

Next, we adjust the parameters of the solid model, defined in Eqs. (6)—(9), again in the same way as in the nitrogen case. It turns out to be fairly easy to adjust ψ_0 and ψ_1 so that $p(x)$ can be subsequently fitted to the envelope with satisfactory accuracy. It seems that $p(x)$ is not as asymmetric as in the nitrogen case. As a result, the pole in $p(x)$, see Eq. (9), is unnecessary and we set $p_s=0$.

With a typical choice of the parameters, $n_2^*(T)$ is increasing (by construction) from 0.96 at 80 K to 0.99 at 95 K. The result for the final choice of parameters is shown in Fig. 9. The two-phase specific heat $C_{||}(n_2^*,T)$ for this choice of parameters is shown in Fig. 11 and is typical of what one obtains with other parameter choices. The model is in qualitative agreement with the experiment, though the model curve is somewhat too smooth. We are not concerned about the high-temperature behavior as our model will surely fail for high enough temperatures.

We now consider the final results shown in Figs. 8—10. These correspond to the following parameters: $T_c=74$ K, $T_0=86$ K, $n_c=0.49$, $\psi_{0,0}=-70.2$ K, $\psi_{0,1}=0.15$, $\psi_{0,2}=-0.011$ K^{-1}, $\psi_{1,0}=-25.5$ K, $\psi_{1,1}=-11.5$, $\psi_{1,2}=0.08$ K^{-1}, $x_m=-0.0345$, $p_2=3.32\times 10^3$ K, $p_3=1.15\times 10^4$ K, $p_4=3.87\times 10^5$ K, and $p_s=0$.

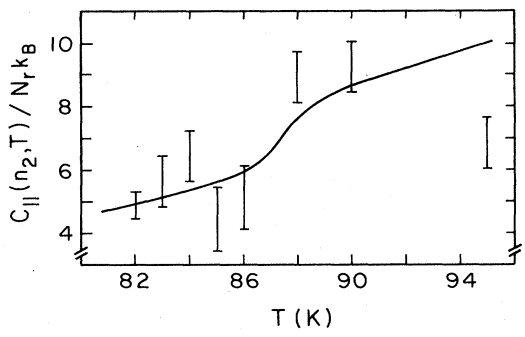

FIG. 11. The two-phase specific heat along the solid-to-coexistence phase boundary. The bars are obtained by extrapolating the experimental two-phase result up to $n=n_2^*$. The solid curve is the model result.

The phase diagram in Fig. 9 is consistent with the experimental information. At the highest temperatures the model predicts values for the coexistence-to-fluid boundary n_1 which are somewhat too low. Analogous behavior was observed for nitrogen. At low temperatures a slightly steeper $n_1(T)$ might be in better agreement with the experiment. Also, the slope of the two-phase specific heat $-\partial C_{||}/\partial n = Td^2\mu_{||}/dT^2$ in Fig. 10 is consistent with experiment, except at the highest temperatures.

Consider next the specific-heat traces in Fig. 8. At low coverages the model gives much sharper peaks at the transition than what is measured. We think that below half a monolayer the difference between the model and the experiment is mainly due to the expected rounding of the experimental data induced by substrate and instrumental effects, rather than due to deficiences of the model. At higher coverages, however, the model seems to overestimate the specific heat above 86 K. This is quite similar to what was observed in the case of nitrogen, see Fig. 2.

At $n=0.919$ the model predicts a maximum of the specific heat at a somewhat lower temperature than experimentally observed. At $n=0.966$ the transition from solid to coexistence is located at 84 K, which is a lower temperature than we inferred earlier on the basis of the dashed line in the figure. Obviously the good agreement of the model with the experiment at this coverage is, to some extent, due to two errors that cancel each other: a shift in the temperature of the phase boundary, and the discrepancy in the heat capacity shown in Fig. 11. Finally, at $n=1.014$ the model does not show any solid-to-coexistence transition (at least not below 96 K). According to the experiment there has to be one below 108 K, but an accurate location cannot be determined from the measured data. The model for the solid, and hence the calculated result at $n=1.014$, should not be taken too seriously.

In summary, the model agrees quite well with the experiment, provided the rounding of the transitions is ignored.

V. INCIPIENT TRIPLE POINT IN GENERAL

In the preceding two sections we have shown that nitrogen and krypton on graphite seem to have an incipient triple point. There is no reason to believe that these two are the only real systems with this behavior. It is therefore of some interest to consider the general thermodynamic properties of such systems, and, in particular, the crossover from an incipient to an ordinary triple point which occurs at a critical endpoint. In this section we consider a simple model of the general type employed above. The general properties of phase boundaries and specific-heat curves in systems close to the critical-endpoint situation are discussed. The qualitative features of the phase diagrams are also apparent in the results of Sander and Hautman.[15]

We employ the following model. The fluid phases are described by the Ising lattice-gas model. The free energy $\phi(n,T)$ of the fluid depends on the critical coverage n_c and the critical temperature T_c. We choose, for simplici-

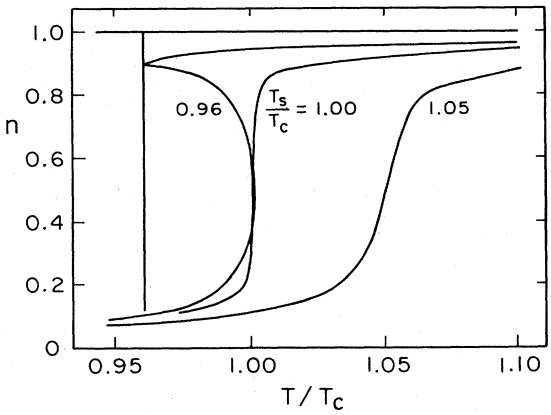

FIG. 12. Submonolayer phase diagrams of model (23), with $a=0.1$ and $T_s/T_c=0.96$, 1.00, and 1.05.

ty, n_c to be equal to half of the monolayer coverage, $n_c=0.5$, so that only T_c is left as a free parameter. It is assumed that the solid has zero specific heat and is completely incompressible, so that the free energy $\psi(n,T)$ of the solid is infinitely large everywhere, except at $n=1.0$, where

$$\psi(n=1,T)=\phi_s+a(T-T_s)\ . \tag{23}$$

Here, $\phi_s=\phi(n_c,T_s)$, a and T_s are the parameters of the solid model, and a has to be chosen large enough so that $\psi(n=1,T)$ increases with temperature relative to $\phi(n_c,T)$.

The ratio T_s/T_c controls the nature of the phase diagram. If $T_s/T_c<1$ an ordinary triple point and a critical point are found, whereas if $T_s/T_c>1$ the phase diagram is of the incipient-triple-point type. If $T_s/T_c=1$ there is a critical endpoint at $T=T_s$. The parameter a is of lesser importance. In Fig. 12 we present three typical phase diagrams corresponding to $T_s/T_c=0.96$, $T_s/T_c=1.00$, and $T_s/T_c=1.05$. We have chosen $a=0.1$ so that the incipient-triple-point case fits conveniently into the figure. Notice that because of our model definition the solid-to-coexistence phase boundary is always at $n=1$.

For $T_s/T_c=0.96$ the phase diagram has, as expected, a triple point at $T=T_s$ and a liquid-gas critical point at $T=T_c$. The case $T_s/T_c=1.05$ is an incipient triple point of the type discussed above for nitrogen and krypton on graphite. For $T_s/T_c=1.00$ there is no liquid phase and the lower phase boundary is quite steep with an infinite slope at the critical point $n_c=0.5$. There is no reason to expect n_1 to be symmetric with respect to the inflection point at $T=T_c$ and $n=n_c$, although the result in Fig. 12 happens to be quite close.

In Fig. 13 we depict the specific heat at constant coverage for the three value of T_s/T_c discussed above. Figure 13(a) corresponds to the incipient-triple-point case. The specific heat is quite similar to the experimental results for nitrogen and krypton on graphite (Secs. III and IV). Below roughly half a monolayer the specific heat has a sharp peak. The height of the peak increases with coverage but always remains finite. Above half a monolayer or

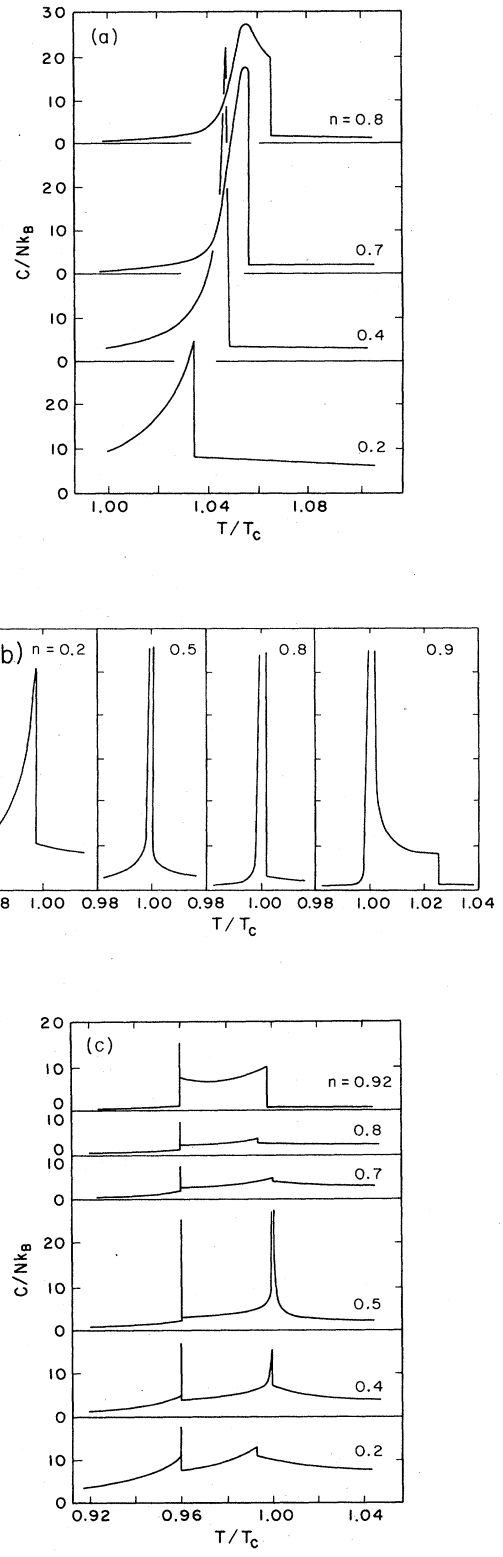

FIG. 13. Specific heat per atom at some fixed coverages, with the same parameters as in Fig. 12. (a) $T_s/T_c=1.05$. (b) $T_s/T_c=1.00$. The specific heat is infinite for $n\geq 0.5$ at the critical endpoint. (c) $T_s/T_c=0.96$. The specific heat is a Dirac delta function at the triple-point temperature.

so the peak is rounded and its height starts to decrease. At high coverages the specific heat has a "shoulder" on the high-temperature side of the peak.

Figure 13(b) corresponds to the critical endpoint $T_s = T_c$. The specific heat diverges at $T = T_s = T_c$ when coverage is larger than $n_c = 0.5$. As coverage is increased the specific-heat peaks become steeper on the low-temperature side. This is quite different from the behavior in Fig. 13(a). On the high-temperature side at sufficiently large coverage the two-phase specific heat again has a "shoulder."

For T_s/T_c less than 1 there is both a triple point and a critical point [Fig. 13(c)]. The logarithmic singularity in the specific heat at the critical point is much weaker than the singularity at the critical endpoint. There are rather small discontinuities in the specific heat at the phase boundaries of the liquid-gas coexistence region, even close to the critical point. Most of the area under the specific-heat peaks in Figs. 13(a) and 13(b) is now compressed under the delta-function peak at the triple point. The qualitative difference between the peaks in Figs. 13(a) and 13(c) is quite similar to that found experimentally in comparing nitrogen and methane on graphite. Specific heats as large as $80k_B$ per molecule are measured at the incipient triple point of nitrogen[5] (Fig. 2), whereas at most $10k_B$ per molecule is observed at the liquid-gas phase boundaries of methane[10] when a smooth background is subtracted off.

VI. CONCLUSIONS

We have devised an internally consistent model of the incipient triple point that gives a complete description of the thermodynamics in the region of interest. The model parameters are adjusted to fit the measured specific heat of nitrogen and krypton adsorbed on graphite, and the model is found to be consistent with the data. In particular, the measured specific-heat data are reproduced quite accurately if the rounding at the transitions from one to two-phase regions is ignored, except in the regime of high coverage and temperature. In that regime it is plausible that the quantitative discrepancies are due to the intrinsic limitations of the lattice-gas model of the fluid phase and do not signal the failure of the incipient-triple-point interpretation. The experimental phase boundaries of the coexistence region are reproduced within the experimental uncertainty at temperatures below roughly 55 K for nitrogen and 94 K for krypton. Above these temperatures the model is no longer reliable.

The basic conclusion of our study, that the experimental data are consistent with the incipient-triple-point model, does not seem to be affected by the nonideality of the substrates used in the experiments. In the case of nitrogen, the fits of the fluid model to the two available sets of experimental data yield basically the same parameters. The mean-field and van der Waals approximations for the fluid phase are less consistent with the experimental data than a two-dimensional Ising lattice gas. This suggests that the agreement of the model with the data is nontrivial.

The incipient-triple-point interpretation of nitrogen and krypton on graphite is supported by the fact that there is a well-defined physical mechanism which explains how the incipient triple point can arise when the corrugation of the adsorption potential favors the commensurate solid phase. The density-functional calculations of Sander and Hautman[15] indicate that the corrugation on graphite is strong enough to lower the free energy of the commensurate solid phase of nitrogen and krypton by an amount sufficient to produce an incipient triple point.

The model parameters we find are consistent with the physical mechanism. The metastable liquid-gas critical temperature of the model is, when properly scaled, close to the experimental estimates of critical temperatures of adsorbed systems that exhibit a genuine critical point. We infer that it is indeed the properties of the solid phase that are the reason for the difference in the behavior of nitrogen and krypton, on the one hand, and xenon and methane, on the other hand, when these are adsorbed on graphite. In units of the critical temperature T_{3c} of the three-dimensional bulk material, our estimates of $T_c = 41$–42 K for nitrogen and $T_c = 72$–78 K for krypton correspond to $T_c = 0.33T_{3c}$ and $T_c = (0.35$–$0.38)T_{3c}$, respectively.[26] For argon,[27] neon,[28] and methane[10] the best experimental estimates are $T_c = 0.36T_{3c}$, and for xenon,[7] $T_c = 0.40T_{3c}$.

The existence of a genuine triple point, in contrast to an incipient triple point, for nitrogen and krypton adsorbed on graphite, is inconsistent with the experimental data. If there were a triple point we would expect to see a very narrow specific-heat peak, as is seen in xenon[9] or methane[10] on graphite. Instead, a much broader peak is observed, and the qualitative difference should not be due to experimental complications.[29] There is also no indication of liquid-gas phase separation as such in krypton or nitrogen on graphite, even though in the case of the nitrogen experiment, at least, the sensitivity should have been sufficient to detect it. In addition, in the case of krypton there is no evidence of liquid-gas phase separation in the vapor-pressure isotherms of Larher.[8]

Another alternative to an incipient triple point for these cases is a tricritical point smeared out by various effects, as proposed by Ostlund and Berker.[16] In favor of their interpretation is the fact that their calculation starts with realistic (or at least plausible) interatomic potentials and does not rely on adjustable parameters in order to predict the basic phase diagram for the system on an ideal substrate. On the other hand, the same authors showed in a later calculation[30] that small changes in the parameters of their lattice-gas model can also lead to a phase diagram of the incipient triple-point variety. Hence it is not inconceivable that a somewhat different choice of interatomic potentials or a different set of approximations in their original calculation could have led to an incipient triple point for krypton or nitrogen on graphite. Indeed, using a rather different theoretical approach, but one which is also based to some extent on interatomic potentials, Sander and Hautman[15] have come to the conclusion that an incipient triple point (in our terminology) occurs for these two cases.

In this paper we have considered the incipient-triple-

point picture in the two special cases of nitrogen and krypton on graphite. The physical mechanism, however, is quite general and we thus expect there will also be other systems with this behavior. In particular, an incipient triple point may occur in some films adsorbed on lamellar halides.[31] The corrugation of the adsorption potential on lamellar halides is stronger than that on graphite, and therefore the commensurate solid phases can have an even lower free energy than on graphite. The crossover from an ordinary to an incipient triple point may be observed in adsorbed films of binary mixtures where the effective size of the adsorbed species can be varied. Bohr *et al.*[32] have found some evidence of an incipient triple point in mixtures of argon and xenon adsorbed on graphite.

It would be interesting to study in more detail under what circumstances a commensurate solid phase is stable enough to give rise to an incipient triple point. In particular, we would like to understand how the corrugation of the adsorption potential and the mismatch between the size of the adsorbed species and the substrate lattice affects the phase diagram of adsorbed films.

ACKNOWLEDGMENTS

We thank M. H. W. Chan, R. M. Suter, A. D. Migone, and N. J. Colella for useful discussions. The financial support received from the Jenny and Antti Wihuri Foundation, the Finnish Cultural Foundation, and the Emil Aaltonen Foundation is gratefully acknowledged by K.J.N. This research was supported by the National Science Foundation through Grant No. DMR-81-08310. This paper is based upon a dissertation submitted by K.J.N. in partial fulfillment of the requirements for the degree of Doctor of Philosophy at Carnegie-Mellon University.

APPENDIX: THE APPROXIMATION TO THE TWO-DIMENSIONAL ISING MODEL

We use the variational real-space renormalization-group method introduced by Kadanoff[20,21] to generate the thermodynamic properties of the Ising model. The calculation consists of iterating the couplings of a plaquette of four spins, and the same recursion relations can be applied for the Ising model on both square and triangular lattices.[33] The only difference between the two cases is in the Hamiltonian that is used to initiate the iteration.

For the square lattice it has been shown[34] that the best accuracy is obtained if every other spin of the original lattice is decimated first, before applying the renormalization group. This exact transformation leads to the Hamiltonian

$$-\beta H = v(m) = hm/4 + \ln[2\cosh(K_{\rm NN}m + h)] \quad \text{(A1)}$$

for each plaquette, where $K_{\rm NN}$ is the nearest-neighbor coupling of the original square lattice, h the magnetic field (both divided by temperature), and m the sum of the spins at the corners of the plaquette:

$$m = \sigma_1 + \sigma_2 + \sigma_3 + \sigma_4 . \quad \text{(A2)}$$

The total Hamiltonian of the system is just a sum over all plaquettes.

For the triangular lattice the results of Southern[33] suggest that best accuracy is obtained if the triangular lattice is treated as a square lattice with (locally) anisotropic next-nearest-neighbor bonds. The initial Hamiltonian is then given by

$$v(m) = hm/4 + K_{\rm NN}(m^2 - 4)/4 . \quad \text{(A3)}$$

In the renormalization-group calculation the Hamiltonian $v(m)$ is iterated. In practice, $v(m)$ is rewritten[34] as

$$v(m) = \sum_{i=1}^{4} K_i s_i(m) , \quad \text{(A4)}$$

where $s_1 = m$ [cf. Eq. (A2)], $s_2 = \sigma_1\sigma_2$ plus permutations, $s_3 = \sigma_1\sigma_2\sigma_3$ plus permutations, $s_4 = \sigma_1\sigma_2\sigma_3\sigma_4$, and $\sigma_1, \sigma_2, \sigma_3, \sigma_4$ are the spins at the corners of the plaquette. The recursion relations are then written for the couplings K_i.

Instead of optimizing the free parameter p of the transformation separately at each iteration as Kadanoff originally suggested, we have decided to use a single expression for p as a function of the coupling K_2 [cf. Eq. (A4)] only. The functional form is adjusted so that the overall accuracy is reasonable. The following form is found to be sufficiently flexible:

$$p(K_2) = A_1 K_2 + A_2 (K_2)^{1/2} \exp(-A_3 K_2) . \quad \text{(A5)}$$

The two terms are sufficient to ensure qualitatively correct behavior at the low- and high-temperature limits (e.g., positive specific heat). In the case of the square lattice we have found that the values $A_1 = 4.7$, $A_2 = 0.86$, and $A_3 = 10$ give reasonable accuracy for the thermodynamic properties.

The above choice of $p(K_2)$, and indeed any choice, gives the critical point slightly displaced from the exact value for the square lattice. Therefore an effective nearest-neighbor coupling $K_{\rm NN}^{\rm eff}$ is used in the initial Hamiltonian (A1) in place of $K_{\rm NN}$. We have adopted the following form:

$$K_{\rm NN}^{\rm eff} = K_{\rm NN} + \Delta K_{\rm NN} \exp[-(K_{\rm NN} - K^*)^2/K_0^2] \times \exp(-h^2/h_0^2) , \quad \text{(A6)}$$

with $\Delta K_{\rm NN} = 0.017$ and $K^* = 0.4576$. The widths are $K_0 = 0.05$ and $h_0 = 0.12$. Note that for these values $K_{\rm NN}^{\rm eff}$ is a monotonic function of $K_{\rm NN}$.

The accuracy of various quantities calculated for the square lattice using the bond-moving method was estimated by comparing these results with information from exact series expansions,[35] the Tarko and Fisher approximants[36] for the susceptibility, and the numerical values of Gartenhaus.[37] The errors are not serious (typically a few percent), except for the susceptibility and the temperature

derivative of the magnetization in small fields below the critical temperature. The inaccuracies do not affect our model fits at temperatures well above the critical one.

For the triangular lattice the best results seem to correspond to $A_1=5.1$, $A_2=0.73$, and $A_3=10$ in Eq. (A5). The critical point is again slightly displaced from its exact value, and thus the effective nearest-neighbor coupling K_{NN}^{eff} of Eq. (A6), with $\Delta K_{NN}=0.003$, $K^*=0.2777$, $K_0=0.05$, and $h_0=0.12$, is used in place of K_{NN} in the initial plaquette Hamiltonian, Eq. (A3). The accuracy of the thermodynamic functions is basically comparable to that for the square lattice, though the inaccuracies on the low-temperature side seem to extend somewhat further away from the critical point.

[1]J. G. Dash, *Films on Solid Surfaces* (Academic, New York, 1975).

[2]*Ordering in Two Dimensions,* edited by S. K. Sinha (North-Holland, Amsterdam, 1980).

[3]*Phase Transitions in Surface Films,* edited by J. G. Dash and J. Ruvalds (Plenum, New York, 1980).

[4]D. M. Butler, J. A. Litzinger, G. A. Stewart, and R. B. Griffiths, Phys. Rev. Lett. **42**, 1289 (1979).

[5]A. D. Migone, M. H. W. Chan, K. J. Niskanen, and R. B. Griffiths, J. Phys. C **16**, L1115 (1983).

[6]M. H. W. Chan, A. D. Migone, K. D. Miner, and Z. R. Li, Phys. Rev. B **30**, 2681 (1984).

[7]A. Thomy and X. Duval, J. Chim. Phys. Phys.-Chim. Biol. **67**, 1101 (1970).

[8]Y. Larher, J. Chem. Soc. Faraday Trans. I **70**, 320 (1975).

[9]J. A. Litzinger and G. A. Stewart, in *Ordering in Two Dimensions,* edited by S. K. Sinha (North-Holland, Amsterdam, 1980).

[10]H. K. Kim and M. H. W. Chan, Phys. Rev. Lett. **53**, 179 (1984).

[11]M. D. Chinn and S. C. Fain, Jr., Phys. Rev. Lett. **39**, 146 (1977).

[12]E. D. Specht, M. Sutton, R. J. Birgeneau, D. E. Moncton, and P. M. Horn, Phys. Rev. B **30**, 1589 (1984).

[13]J. K. Kjems, L. Passell, H. Taub, and J. G. Dash, Phys. Rev. Lett. **32**, 724 (1974).

[14]R. D. Diehl, M. F. Toney, and S. C. Fain, Jr., Phys. Rev. Lett. **48**, 177 (1982).

[15]L. M. Sander and J. Hautman, Phys. Rev. B **29**, 2171 (1984).

[16]S. Ostlund and A. N. Berker, Phys. Rev. Lett. **42**, 843 (1979).

[17]T. T. Chung and J. G. Dash, Surf. Sci. **66**, 559 (1977).

[18]D. K. Fairobent, W. F. Saam, and L. M. Sander, Phys. Rev. B **26**, 179 (1982).

[19]J. R. Klein, M. H. W. Chan, and M. W. Cole, Surf. Sci. **148**, 200 (1984).

[20]L. P. Kadanoff, Phys. Rev. Lett. **34**, 1005 (1975).

[21]L. P. Kadanoff, A. Houghton, and M. C. Yalabik, J. Stat. Phys. **14**, 171 (1976).

[22]A. D. Migone, Ph.D. dissertation, Pennsylvania State University, 1984 (unpublished).

[23]M. H. W. Chan (private communication).

[24]T. T. Chung, Ph.D. dissertation, University of Washington, 1976 (unpublished).

[25]D. M. Butler, Ph.D. dissertation, University of Pittsburgh, 1979 (unpublished).

[26]The analysis of Sander and Hautman (Ref. 15) yields somewhat higher values (45 and 84 K). However, these estimates are based on the early Monte Carlo simulations, which apparently overestimated the critical temperature by perhaps 5%. In addition, the values depend on the strength ϵ of the Lennard-Jones interaction of the adsorbed species. The proper values of ϵ are still slightly uncertain and, in fact, even the very form of the Lennard-Jones potential may not be appropriate in the case of adsorbed systems (Ref. 19).

[27]A. D. Migone, Z. R. Li, and M. H. W. Chan, Phys. Rev. Lett. **53**, 810 (1984).

[28]R. E. Rapp, E. P. de Souza, and E. Lerner, Phys. Rev. B **24**, 2196 (1981).

[29]The nitrogen (Ref. 6) and methane (Ref. 10) experiments were performed with basically the same substrate and the same technique; similarly, the technique and substrate were essentailly the same for the krypton (Ref. 4) and xenon (Ref. 9) experiments.

[30]S. Ostlund and A. N. Berker, Phys. Rev. B **21**, 5410 (1980).

[31]F. Millot, Y. Larher, and C. Tessier, J. Chem. Phys. **76**, 3327 (1982).

[32]J. Bohr, M. Nielsen, J. Als-Nielsen, K. Kjaer, and J. P. McTague, Surf. Sci. **125**, 181 (1983).

[33]B. W. Southern, J. Phys. A **11**, L1 (1978).

[34]T. W. Burkhardt, Phys. Rev. B **13**, 3187 (1976).

[35]C. Domb, in *Phase Transitions and Critical Phenomena,* edited by C. Domb and M. S. Green (Academic, New York, 1974), Vol. 3.

[36]H. B. Tarko and M. E. Fisher, Phys. Rev. B **11**, 1217 (1975).

[37]S. Gartenhaus, Phys. Rev. B **27**, 1698 (1983).